# Defining Electronic Excited States Using Time-Resolved Infrared Spectroscopy and Density Functional Theory Calculations†

**Dana M. Dattelbaum,*,‡ Kristin M. Omberg,‡,§ P. Jeffrey Hay,⊥ Nouvelle L. Gebhart,⊥ Richard L. Martin,⊥ Jon R. Schoonover,*,‡ and Thomas J. Meyer||**

*Materials Science and Technology and Theoretical Divisions and the Associate Director for Strategic Research, Los Alamos National Laboratory, Los Alamos, New Mexico 87545*

*Received: October 13, 2003; In Final Form: February 10, 2004*

Characteristic patterns of infrared bands in the $\nu$(CO) region have been observed in the time-resolved infrared (TRIR) spectra of *fac*-rhenium tricarbonyl complexes that allow for identification of transient states that result following laser flash excitation. These patterns can be interpreted by combining experimental TRIR data with density functional theory (DFT) calculations. The DFT calculations are particularly valuable as they provide vibrational energy shifts between the ground and excited states and an analysis of the electronic interactions in terms of the orbitals involved in the excitation. TRIR and DFT results for four different transient excited states, intraligand $\pi \rightarrow \pi^*$, metal-to-ligand charge transfer (MLCT), intramolecular (d$\pi$−O$\pi$) $\rightarrow \pi^*$ excited states, and a redox-separated (RS state), are presented here. A unique example of competing excited states studied by TRIR is also presented. The complexes studied include *fac*-[Re$^{I}$(CO)$_3$(Me$_2$dppz)(4-Etpy)]$^+$, *fac*-[Re$^{I}$(CO)$_3$(bpy)(4-Etpy)]$^+$, *fac*-[Re$^{I}$(CO)$_3$(4,4′-(CH$_3$)$_2$bpy)(OQD)] , *fac*-[Re$^{I}$(CO)$_3$(Me$_2$dppz)(py-PTZ)]$^+$, and *fac*-[Re$^{I}$(CO)$_3$(dppz)(py-PTZ)]$^+$ (Me$_2$dppz is dimethyl dipyrido[3,2-*a*:2′,3′-*c*]phenazine; dppz is dipyrido-[3,2-*a*:2′,3′-*c*]phenazine; 4Etpy is 4-ethylpyridine; bpy is 2,2′-bipyridine; 4,4′-(CH$_3$)$_2$bpy is 4,4′-(CH$_3$)-2,2′-bipyridine; OQD is 1-methyl-6-oxyquinone; py-PTZ is 10-(4-picolyl)phenothiazine). In addition to the DFT studies on the lowest triplet states probed by TRIR spectroscopy, time-dependent DFT (TD-DFT) calculations were also performed to analyze several of the lowest singlet and triplet excited states for each of the complexes.

## Introduction

Rhenium polypyridyl complexes of the type *fac*-[Re$^{I}$(CO)$_3$(pp)(L)]$^{n+}$ (where pp = a bidentate polypyridyl ligand, e.g. 2,2′-bipyridine, L is a monodentate N- or O-bound ligand or a halide (X), and *n* depends on the charge type of L) have been widely used in studies of photoinduced electron and energy transfer.[1−17] Their facile preparation, combined with synthetically tunable ground- and excited-state redox properties, make them excellent systems for photophysical studies. These complexes were also among the first to be studied by time-resolved infrared (TRIR) spectroscopy.[1,6,18−23] The $\nu$(CO) stretching vibrations have high oscillator strengths and are sensitive to changes in electronic structure at the metal due to strong metal−ligand d$\pi$(Re)−$\pi^*$(CO) interactions. TRIR measurements in the $\nu$(CO) region give insight into differences in electronic structure between ground- and excited-state(s) since the band energies are affected by changes in electron density and the associated orbital interactions.

There is currently a large body of TRIR data on facial rhenium tricarbonyl systems, and characteristic patterns have been observed in the spectra that allow for easy identification of an undefined transient state by fingerprinting.[18,21] These patterns can be interpreted by combining group theory and excited-state electronic interactions, consistent with early analyses of the IR spectra of carbonyl complexes.[24−29] Likewise, recent approaches using density functional theory (DFT) calculations have been useful in describing ground-state properties in inorganic complexes.[30] More recently, the application of DFT and time-dependent DFT has led to multiple and informative studies on excited states of transition metal complexes. [31−35] Here, we present the results of an in-depth study of the electronic nature of various excited states in *fac*-Re tricarbonyl polypyridyl complexes using time-resolved infrared spectroscopy combined with density functional theory calculations. In this paper, TRIR spectra of *fac*-[Re$^{I}$(CO)$_3$(bpy)(4-Etpy)]$^+$ (**1**), *fac*-[Re$^{I}$(CO)$_3$(4,4′-(CH$_3$)$_2$bpy)(OQD)] (**2**), *fac*-[Re$^{I}$(CO)$_3$(Me$_2$dppz)(4-Etpy)]$^+$ (**3**), *fac*-[Re$^{I}$(CO)$_3$(Me$_2$dppz)(py-PTZ)]$^+$ (**4**), and *fac*-[Re$^{I}$(CO)$_3$(dppz)(py-PTZ)]$^+$ (**5**) are presented and interpreted with the aid of DFT calculations on a manifold of frontier molecular orbitals in these complexes. This analysis points to the existence of four different electronic origins in this series of complexes − MLCT, putative (d$\pi$−O$\pi$) $\rightarrow \pi^*$, intraligand $\pi \rightarrow \pi^*$ excited states, and a redox-separated (RS) state. Structures for the complexes are shown in Figure 1.

## Experimental Section

**Materials.** Acetonitrile and 1,2-dichloroethane were purchased from Aldrich and used without further purification. *fac*-[Re$^{I}$(CO)$_3$(Me$_2$dppz)(4-Etpy)](PF$_6$), *fac*-[Re$^{I}$(CO)$_3$(bpy)(4-Etpy)](PF$_6$),[11,12] *fac*-[Re$^{I}$(CO)$_3$(Me$_2$dppz)(py-PTZ)](PF$_6$),[11,36] and *fac*-[Re$^{I}$(CO)$_3$(4,4′-(CH$_3$)$_2$bpy)(OQD)](PF$_6$)[37] (Me$_2$dppz is dimethyl

* Corresponding authors. E-mail: (J.R.S.) schoons@lanl.gov; (D.M.D.) danadat@lanl.gov.

† This manuscript is dedicated to the memory of Nouvelle L. Gebhart.

‡ Materials Science and Technology Division, Los Alamos National Laboratory.

§ Current address: Decisions Applications Division, Los Alamos National Laboratory.

⊥ Theoretical Division, Los Alamos National Laboratory.

|| Associate Director for Strategic Research, Los Alamos National Laboratory.

10.1021/jp037096e CCC: $27.50 
Published on Web 03/23/2004

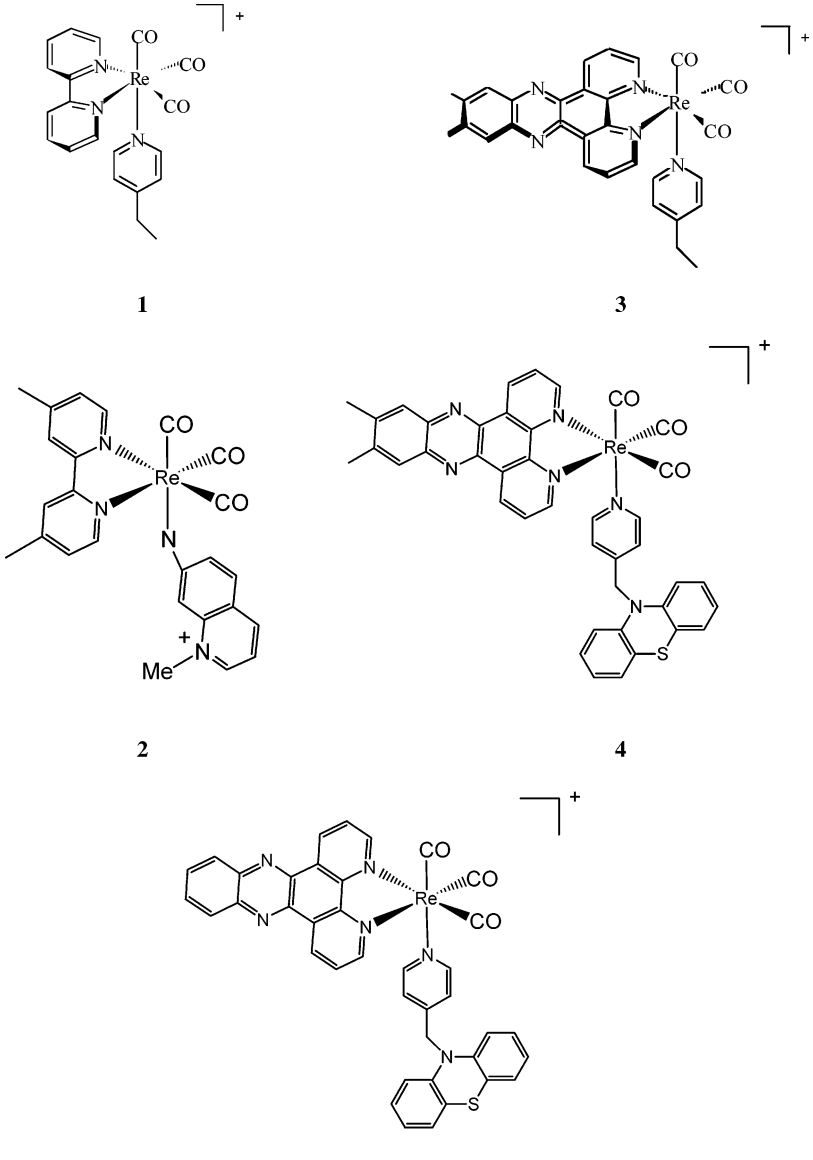


**Figure 1.** Structures of the complexes used in this study: *fac*-[$Re^{I}(CO)_3$(bpy)(4-Etpy)]$^+$ (**1**), *fac*-[$Re^{I}(CO)_3$(4,4′-$(CH_3)_2$bpy)(OQD)] (**2**), *fac*-[$Re^{I}(CO)_3(Me_2dppz)$(4-Etpy)]$^+$ (**3**), *fac*-[$Re^{I}(CO)_3(Me_2dppz)$(py-PTZ)]$^+$ (**4**), and *fac*-[$Re^{I}(CO)_3$(dppz)(py-PTZ)]$^+$ (**5**).

dipyrido[3,2-*a*:2′,3′-*c*]phenazine; 4-Etpy is 4-ethylpyridine; bpy is 2,2′-bipyridine; py-PTZ is 10-(4-picolyl)phenothiazine; 4,4′-$(CH_3)_2$bpy is 4,4′-$CH_3$-2,2′-bipyridine; OQD is 1-methyl-6-oxyquinone) were prepared according to literature procedures.

A modification of the literature procedure was used to prepare *fac*-[$Re^{I}(CO)_3(Me_2dppz)$(py-PTZ)]($PF_6$).[38,39] To a stirring solution of 53 mg (0.075 mmol, 1 equiv) of *fac*-[$Re^{I}$(dppz)$(CO)_3$-(OTf)] ($OTf^-$ is the triflate ion) in 12 mL of degassed methanol was added 41.6 mg of py-PTZ (0.143 mmol, 1.9 equiv). The mixture was heated to reflux with stirring for 2.5 h under argon in the dark. Seven milliliters of aqueous saturated $NH_4PF_6$ was added, and the solution was cooled to 0° C in an ice bath. The desired salt precipitated and was collected via suction filtration and washed with cold $Et_2O$. It was purified twice by redissolving in a minimal amount of $CH_2Cl_2$ and precipitated into cold, swirling isooctane. The precipitate was chromatographed on alumina with 2:1 $CH_3CN$:toluene to yield 29 mg of product (0.03 mmol, 40% yield). Anal. Calculated for $ReC_{39}H_{24}F_6N_6O_3PS$: C, 47.42; H, 2.45; N, 8.51. Found: C, 46.76; H, 2.73; N, 8.47, (possibly residual $NH_4PF_6$). $^1$H NMR ($CD_2Cl_2$): $\delta$ 9.98 (2H; dd, $J$ = 1.3 and 8.2 Hz; $H_1$, $H_8$); 9.58 (2H; dd, $J$ = 1.2 and 5.2 Hz; $H_3$, $H_6$); 8.48 (2H; dd, $J$ = 1.3 and 8.2 Hz; $H_{10}$, $H_{13}$); 8.27 (2H; dd, $J$ = 5.3 and 8.3 Hz; $H_2$, $H_7$); 8.19 (2H; d, $J$ = 6.7 Hz; *2,6-py*-$CH_2$−PTZ); 8.105 (2H; dd, $J$ = 3.4 and 6.6 Hz; $H_9$ and $H_{12}$); 7.31 (2H; d, $J$ = 6.7 Hz; *3,5-py*-$CH_2$−PTZ); 7.05 (2H; dd, $J$ = 1.35 and 7.35 Hz; py-$CH_2$−*PTZ-1,9*); 6.83 (4H; ddd, $J$ = 1.2, 6.6, and 8.0 Hz; py-$CH_2$−*PTZ-2,3,7,8*); 6.41 (2H; d, $J$ = 8.1 Hz; py-$CH_2$−*PTZ-4,6*); and 4.94 (2H; s; py-$CH_2$−PTZ).[38]

**Infrared Measurements.** Infrared measurements utilized either a BioRad FTS 60A/896 or Bruker IFS 66V/s step-scan interferometer with an external Kolmar MCT detector (25 ns rise-time). Both methods have been described previously.[40,41] In both experiments, the IR signal from the detector was amplified and processed by a fast transient digitizer board installed in a Pentium PC. This board also controlled the mirror movement, which was stepped in coordination with the laser pulse operating at 10 Hz for this experiment.

Samples were excited at 355 nm by using the third harmonic of a Nd:YAG laser (Spectra Physics GCR-11, 7 ns pulse width, or Continuum Surelite-II, 5−7 ns pulse width, both operated at 10 Hz). Individual points on the interferogram were collected

**TABLE 1: Experimental and Calculated Ground and Excited State $\nu$(CO) Band Energies and Excited-to-Ground State Shifts ($\Delta\bar{\nu}$) in cm$^{-1}$ in $CH_3CN$ or 1,2-Dichloroethane and Excited State Electronic Origins**

| complex[a] | ground state $\nu$(CO) | calcd | excited state $\nu$(CO) | calcd | $\Delta\bar{\nu}$ | calcd | excited state assignment |
|---|---|---|---|---|---|---|---|
| 1 | 2035 | 2120 | 2074 | 2135 | +39 | +15 | MLCT |
| | 1927 | 2049, 2038 | 2010 | 2093 | +83 | +48 | |
| | | | 1971 | 2060 | +44 | +22 | |
| 2 | 2019 | 2106 | 2023 | 2106 | +4 | 0 | (d$\pi$(Re)−O$\pi$)−$\pi$* |
| | 1909 | 2029 | 1936 | 2048 | +27 | +19 | |
| | 1900 | 2021 | 1928 | 2040 | +28 | +19 | |
| 3 | 2036 | 2117 | 2031 | 2116 | −5 | −1 | $\pi\pi$* |
| | 1932 | 2045, 2034 | 1922 | 2044, 2033 | −10 | −1, −1 | |
| 4 | 2036 | *b* | 2030 | *b* | −6 | *b* | RS |
| | 1934 | | 1915 | | −19 | | |
| 5 | 2037 | *b* | 2028,[b] 2031[c] | *b* | −9,[c] −6[d] | *b* | RS and $\pi\pi$* |
| | 1937 | | 1915,[b] 1919[c] | | −22,[c] −18[d] | | |

[a] Note Figure 1 for complex structures. [b] DFT results not available. [c] Early time data (RS + $\pi\pi$*). [d] Late time data ($\pi\pi$* only).

by the interferometer software every 20−200 ns after the laser pulse for 1 $\mu$s. The data were organized into individual interferograms representing the interferogram at every 200 ns point, then Fourier transformed into spectra. Spectra were averaged between the laser pulse and the transient lifetime to give the final TRIR spectra. Ground- and excited-state spectra shown are an average of 64 or 128 scans.

**Samples for TRIR Studies.** All IR spectra were measured in acetonitrile or 1,2-dichloroethane, in a 0.75 or 1 mm path length sealed $CaF_2$ or $BaF_2$ cell. Sample concentrations were adjusted to give an absorbance of ∼0.7 for the ground state $\nu$(CO) bands. The sample cell and sample solutions were deoxygenated by sparging with argon for 15 min. Solutions were transferred to the sample cell under an inert atmosphere. Spectra were acquired in blocks of 32 scans to prevent sample decomposition.

**Calculations**. The hybrid B3LYP DFT approximation,[42a] as implemented in Gaussian98,[42b] was used to determine the geometry and vibrational frequencies of the ground singlet state and lowest triplet state of the $Re(CO)_3(pp)(L)^+$ complexes. The shifts in the calculated carbonyl frequencies in the triplet state relative to the ground state were then calculated to compare to the experimental TRIR spectra. Rhenium was described by the LANL2 relativistic effective core potential and associated basis set,[43] which was uncontracted as discussed previously.[34] The 6-31G* basis sets were employed for the ligands.

Excited singlet and triplet states were calculated at the calculated ground-state geometry using time-dependent DFT (TDDFT) calculations also employing the B3LYP functional.[43−45] The absolute error in DFT calculations is ∼ 4% compared to the ∼15% typically observed in previous generation calculations such as Hartree−Fock. Some of this error is due to the lack of solvent effects in the calculations.

## Results

**Ground- and Excited-State Spectra.** A summary of ground and time-resolved infrared $\nu$(CO) frequencies is given in Table 1 for complexes **1**−**5**. The experimental and calculated (when available) carbonyl mode frequencies are given, along with the energy shifts of the carbonyl modes between ground and excited state, $\Delta\nu = \nu_{es} - \nu_{gs}$. Representative examples of ground and time-resolved infrared spectra are given in Figures 2 and 3. For brevity, TRIR results for remaining complexes are listed in Table 1. Table 2 details calculated and experimental transition energies. The agreement between DFT-calculated transition energies and experimental values is particularly notable.

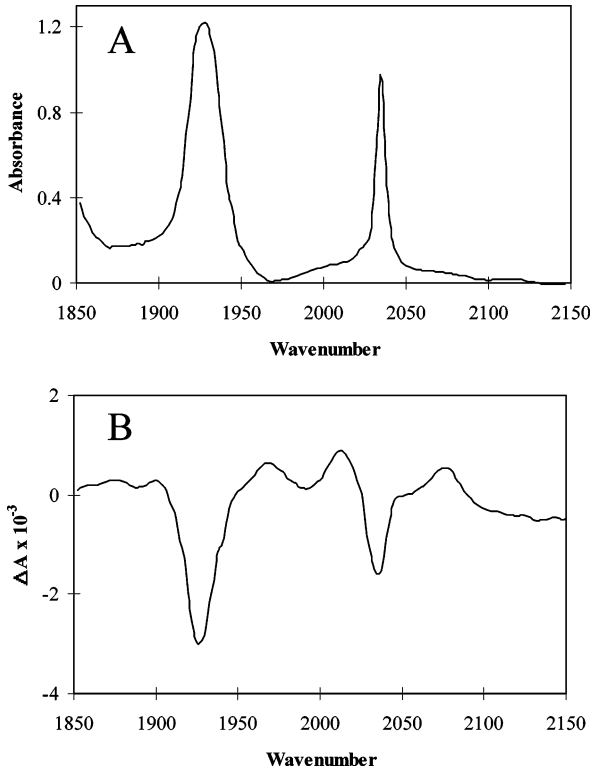


**Figure 2.** Ground-state (A) and TRIR (B) spectra of *fac*-$[Re(CO)_3(bpy)(4\text{-}Etpy)]^+$ between 1850 and 2150 cm$^{-1}$ at 298 K in $CH_3CN$.

The ground-state (A) and TRIR (B) spectra of *fac*-$[Re(CO)_3(bpy)(4\text{-}Etpy)]^+$ (**1**) shown in Figure 2 have been extensively discussed in the previous paper.[34] Two $\nu$(CO) bands appear in the ground-state spectrum; a narrow band at 2035 and a broad band centered at 1927 cm$^{-1}$. The broad band is the unresolved superposition of two $\nu$(CO) bands consistent with effective $C_{3v}$ symmetry with three pyridyl-type ligands occupying facial coordination sites. The excited-state spectrum exhibits broad $\nu$(CO) bands at 2074, 2010, and 1971 cm$^{-1}$ shifted substantially to higher energy compared to the ground state. The appearance of three resolved bands is consistent with a lowering of local symmetry due to electron occupation of the bpy ligand. This complex has a lowest-lying MLCT excited state(s), and the pattern of large, positive band shifts in the TRIR spectrum is a characteristic feature.[5,15,17]

The ground-state (A) and TRIR (B) spectra of complex **2**, *fac*-$[Re(CO)_3(bpy)(OQD)]$, in acetonitrile, at 298 K in the carbonyl region are shown in Figure 3. The ground-state spectrum, Figure 3A, exhibits three $\nu$(CO) bands, one narrow

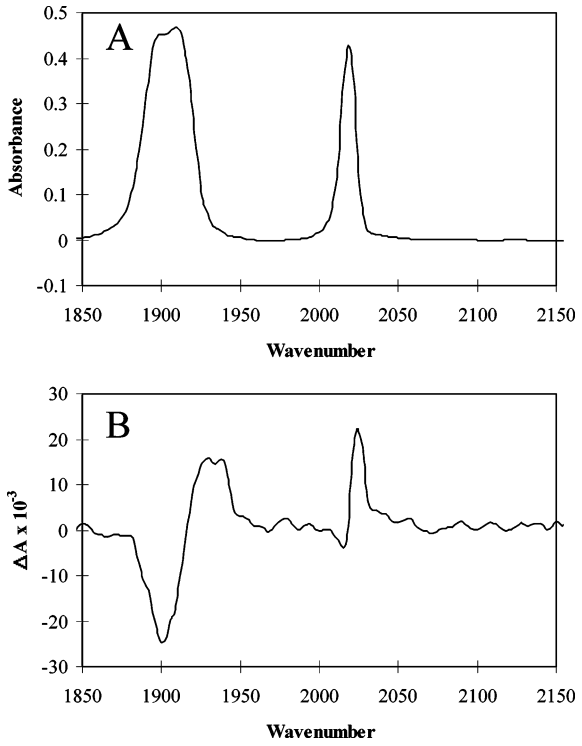


**Figure 3.** Ground-state (A) and TRIR (B) spectra of *fac*-[Re(CO)$_3$-(4,4′-(CH$_3$)$_2$bpy)(OQD)]$^+$ between 1850 and 2150 cm$^{-1}$ at 298 K in CH$_3$CN.

**TABLE 2: Summary of TDDFT Calculations on Re(CO)$_3$(bpy)(L)$^+$ Complexes**

| | E(eV) | | | | |
|---|---|---|---|---|---|
| state | calcd | expt | orbital excitation | designation | f |
| | | | pp = bpy, L = 4-Etpy (**1**) | | |
| $T_1$ | 2.51 | 2.21[b] | $d_1 \rightarrow \pi^*$ bpy | MLCT | |
| $S_1$ | 2.65 | | $d_1 \rightarrow \pi^*$ bpy | MLCT | 0.0097 |
| $T_2$ | 2.70 | | $d_2 \rightarrow \pi^*$ bpy | MLCT | |
| $T_3$ | 2.90 | | $d_3 \rightarrow \pi^*$ bpy | MLCT | |
| $S_2$ | 2.91 | | $d_2 \rightarrow \pi^*$ bpy | MLCT | 0.0057 |
| $S_3$ | 3.02 | | $d_3 \rightarrow \pi^*$ bpy | MLCT | 0.1511 |
| | | | pp = Me$_2$bpy, L = OQD (**2**) | | |
| $T_1$ | 2.02 | ~1.7[a] | $d\pi-O\pi \rightarrow \pi^*$ oqd | $d\pi-O\pi \rightarrow \pi^*$ | |
| $T_2$ | 2.37 | | $d\pi-O\pi \rightarrow \pi^*$ bpy | MLCT | |
| $S_1$ | 2.46 | | $d\pi-O\pi \rightarrow \pi^*$ bpy | MLCT | 0.003 |
| $T_3$ | 2.63 | | $d_1 \rightarrow \pi^*$ bpy | MLCT | |
| $S_2$ | 2.68 | | $d\pi-O\pi \rightarrow \pi^*$ oqd | $d\pi-O\pi \rightarrow \pi^*$ | 0.157 |
| $S_3$ | 2.89 | | $d_1 \rightarrow \pi^*$ bpy | MLCT | 0.080 |

[a] For the complex *fac*-[Re(4,4′-($^t$Bu)$_2$bpy)(CO)$_3$(OQD)].[37] [b] Reference 34.

band at 2019 and two lower energy bands at 1909 and 1900 cm$^{-1}$. The anionic nature of the OQD ligand and its ability as an electron donor compared to 4-ethylpyridine *fac*-[Re(CO)$_3$-(bpy)(4-Etpy)]$^+$ causes the shifts to lower energy. It also lowers the local symmetry which splits the low energy $\nu$(CO) band into two components.

In the time-resolved spectrum, Figure 3B, all three bands are shifted to higher energy relative to the ground state at 2023, 1936, and 1928 cm$^{-1}$. The excited-state shifts are positive as for the MLCT state in **1**, but are smaller in magnitude (+4, +17, +28).

The excited state band energies and ground-to-excited state shifts for the three infrared-active modes are listed in Table 1. It was initially suggested that this pattern of bands is attributable to a (Re−O)$\sigma \rightarrow \pi^*$ excited state; however the DFT calculations suggest another origin (see Discussion).[37,46−48]

Ground-state infrared and TRIR results for *fac*-[Re(Me$_2$dppz)-(CO)$_3$(4-Etpy)]$^+$, **3**, are listed in Table 1. There is evidence that the lowest-lying excited state in this complex is an intraligand $\pi \rightarrow \pi^*$ state localized on Me$_2$dppz.[38,49] For this excited state, ground-to-excited-state shifts in $\nu$(CO) are small and negative suggesting that the ligand-based triplet is a net electron donor in the excited state (Table 1).

Ground-state infrared and TRIR results for *fac*-[Re(Me$_2$dppz)-(CO)$_3$(py-PTZ)]$^+$, **4**, are also reported in Table 1. The lowest-lying excited state in this complex is a redox-separated state, *fac*-[Re(Me$_2$dppz$^{\bullet-}$)(CO)$_3$(py-PTZ$^{\bullet+}$)]$^{+*}$. It is characterized by the appearance of PTZ$^{\bullet+}$ at $\lambda_{max}$ = 510 nm in the transient absorption spectrum[38,39,50] and a transient decay time of $\tau \sim$ 63 ns ($k \sim 2.0 \times 10^7$ s$^{-1}$).[51] In the transient spectrum, $\nu$(CO) bands at 2036 and 1934 cm$^{-1}$ shift to 2030 and 1915 cm$^{-1}$. The local ground-state symmetry is retained in the excited state and the shifts are negative, similar to the $\pi\pi^*$ excited state in *fac*-[Re(Me$_2$dppz)(CO)$_3$(4-Etpy)]$^+$, but are larger in magnitude.

In the ground state of *fac*-[Re(dppz)(CO)$_3$(py-PTZ)]$^+$, **5**, only two CO bands appear (at 2036 and 1932 cm$^{-1}$) as in *fac*-[Re-(Me$_2$dppz)(CO)$_3$(4-Etpy)]$^+$ due to the pseudo-$C_{3v}$ symmetry around the metal center. Time-resolved infrared spectra are shown in Figure 4, parts A and B. There is evidence in the early spectrum of *fac*-[Re$^{\rm I}$(dppz)(CO)$_3$(py-PTZ)]$^+$ of a competition between initially formed $\pi\pi^*$ and redox-separated states following MLCT excitation.[38] The energies of the ground- and excited-state $\nu$(CO) bands are compared in Table 1. Figure 4A is the average of $\Delta$ absorbance spectra averaged over 20−300 ns in dichloroethane at 298 K. In this time regime, both states exist and the spectrum reveals the average negative shifts in the $\nu$(CO) bands (weighted by the relative populations of the two states). At later times, only the $\pi\pi^*$ state remains and the negative shifts in $\nu$(CO) are decreased in magnitude compared to the average in Figure 4A and are similar to those observed for the $\pi\pi^*$ state in **3**. Figure 4B shows TRIR spectra of *fac*-[Re(dppz)(CO)$_3$(py-PTZ)]$^{+*}$ separated into early and late time slice average spectra. At early times (<300 ns, dashed line), the RS dominates, and the pattern of bands observed in the TRIR spectrum is typical for a redox-separated state. The excited-state shifts are in the same direction as those for a $\pi\pi^*$ state, but larger. At later times (>300 ns, solid line), the $\pi\pi^*$ state dominates and the ground-to-excited-state shifts in $\nu$(CO) are smaller compared to the RS state. In essence, there is a contraction of the excited-state band energies toward the ground-state bleach with time due to the changing populations of the two excited states.

**DFT Calculations.** DFT calculations were performed on complexes **1**, **2**, **3**, and **5**. The results for the MLCT state(s) in complex **1** were reported previously.[34,52] Figure 5 shows pictorial representations of the DFT-calculated HOMO and LUMO orbitals for **2** and the associated frontier molecular orbital energy level diagram. The HOMO is a $d\pi-O\pi$ orbital with significant $d\pi$(Re) and $\pi$(O) character. The LUMO is a $\pi^*$ orbital on the OQD ligand with little O character and is primarily localized on the aromatic rings of the ligand. The DFT-calculated ground- and excited-state carbonyl frequencies are compared to the experimental values in Table 1.

The DFT-calculated HOMO and LUMO orbital illustrations for **3** are shown in Figure 6. The HOMO is a $d\pi$(Re)-based orbital. Two closely lying LUMO orbitals are localized on the Me$_2$dppz ligand and are often referred to as the phen (or bpy) and phenazine portions of the ligand. According to the DFT calculations presented here, the phen-localized $\pi^*$ orbital is

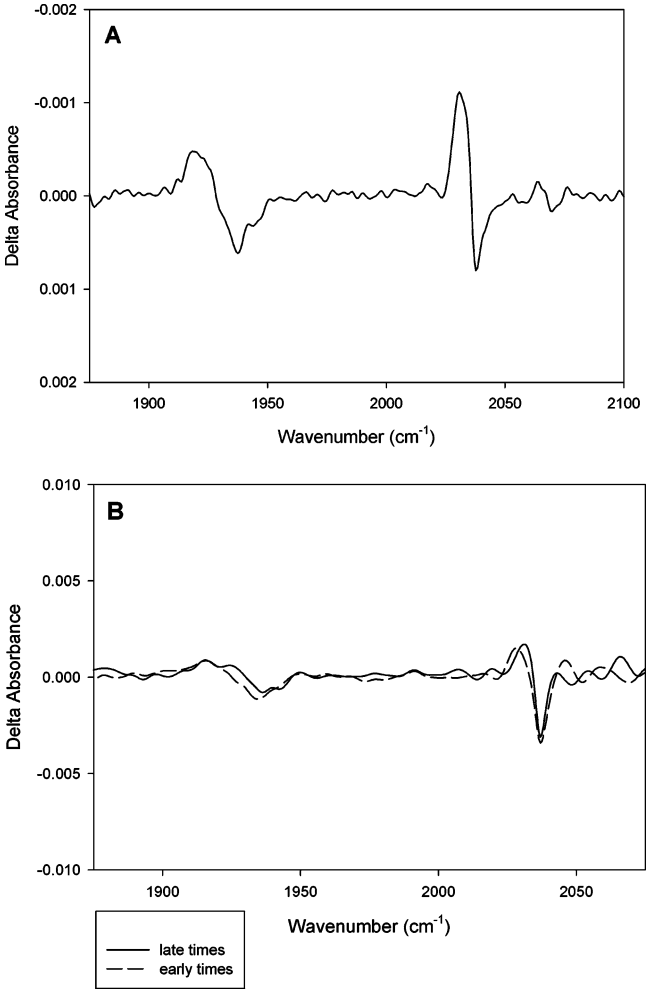


**Figure 4.** (A) TRIR spectrum of *fac*-[Re(dppz)(CO)$_3$(py-PTZ)]$^{+*}$ averaged over early times (20−300 ns) in dichloroethane at 298 K. (B) TRIR spectra of *fac*-[Re(dppz)(CO)$_3$(py-PTZ)]$^{+*}$ separated into early and late time average spectra. At early times (<300 ns, dashed line), the RS dominates. At later times (>300 ns, solid line), the $\pi\pi^*$ state dominates and the ground-to-excited-state shifts in $\nu$(CO) decrease.

slightly lower in energy. The DFT-calculated HOMO and LUMO orbitals for **5,** as shown in Figure 7, are found on the py-PTZ and phen portion of dppz ligands, respectively. The calculated excitation energies from TD-DFT calculations are summarized in Tables 2 and 3.

## Discussion

There is an extensive literature on the ground-state group theory of facial tricarbonyl complexes, dating back over three decades.[24−29] For a complex of type *fac*-[Re$^{I}$(CO)$_3$(pp)(L)]$^{n+}$, there are three CO stretching modes, A′(1), A′(2) and A″. They are shown below:[29]

In complexes in which the ancillary ligand L is pyridine-based (i.e., when L is an N-bound pyridyl ligand) the local coordination environment around the metal center is pseudo-$C_{3v}$ symmetry, and only two bands appear in the ground-state spectrum, an $A_1$ mode at higher energy and a broad band at lower energy (E) that is the convolution of the A′(2) and A″ bands of $C_s$ symmetry. When the ancillary ligand, L, is not a pyridyl ligand, the local symmetry is reduced to $C_s$ and three bands due to the A′(1), A′(2), and A″ modes appear in the infrared spectrum.[53]

Upon photoexcitation to a metal-to-ligand charge-transfer excited state, *fac*-[Re$^{II}$(CO)$_3$(pp$^{\bullet-}$)(L)]$^{n+*}$, the symmetry is lowered to $C_s$ due to the promotion of an electron from the d$\pi$(Re) orbitals to $\pi^*$(pp) and lowering of symmetry. For complexes with $C_s$ ground-state symmetry, there is no formal change in symmetry and the designation of the modes in the excited-state remains the same as in the ground-state spectrum. Complexes with pseudo-$C_{3v}$ ground-state symmetry in the ground state (with an N-bound ligand, L) undergo a symmetry change to $C_s$ upon excitation because of electron occupation of $\pi^*$(pp).

The CO ligand is a strong $\pi$-acid, or $\pi$-acceptor ligand. There is extensive $\pi$-back-bonding between the CO $\pi^*$ orbital and the metal d$\pi$ orbitals. This stabilizes the metal d$\pi$ orbitals, and destabilizes CO $\pi^*$. Variations in d$\pi$(M)−$\pi^*$(CO) back-bonding induced by the changes in the remaining ligands dominate in the ground state. In the excited states, there are three relevant interactions: (1) loss of d$\pi$(M)−$\pi^*$(CO) back-bonding and $\sigma$-(M−C) bond polarization, due to partial oxidation at the metal, (2) $\pi^*$(4,4′−X$_2$bpy$^{\bullet-}$)−$\pi^*$(CO) mixing which provides an orbital basis for mixing $\pi^*$(4,4′−X$_2$bpy$^{\bullet-}$) and $\pi^*$(CO)-based MLCT excited states, and (3) d$\pi$(M)−$\pi$(pp) mixing which provides an orbital basis for mixing MLCT and $\pi\pi^*$ excited states.[34] Through these interactions, the CO stretch is highly convoluted with the metal d$\pi$ electrons, and the energy of the CO stretching frequency is a good indicator of electron density at the metal center. In particular, the results of previous DFT calculations on *fac*-[Re$^{I}$(bpy)(CO)$_3$(4-Etpy)]$^{+*}$ have been revealing and support the importance of $\pi^*$(4,4′−X$_2$bpy$^{\bullet-}$)−$\pi^*$(CO) mixing confirmed by the predicted excited-state structural changes.[34]

On the basis of these qualitative arguments based on metal−CO interactions, the nature of the CO stretch, and the frontier orbitals and the compositions of the normal modes, there are straightforward explanations for the characteristic pattern of bands observed in the TRIR spectra of $\pi \rightarrow \pi^*$, MLCT and d$\pi$−O$\pi \rightarrow \pi^*$ excited states, and redox-separated states. The combination of experimental data, qualitative arguments, and DFT calculations represent a powerful approach for gaining unique insight into these transient states.

**Metal-to-Ligand Charge Transfer (MLCT) Excited States.** The TRIR spectra of MLCT excited states typically exhibit the pattern of bands exhibited by *fac*-[Re(CO)$_3$(bpy)(4-Etpy)]$^{+*}$,

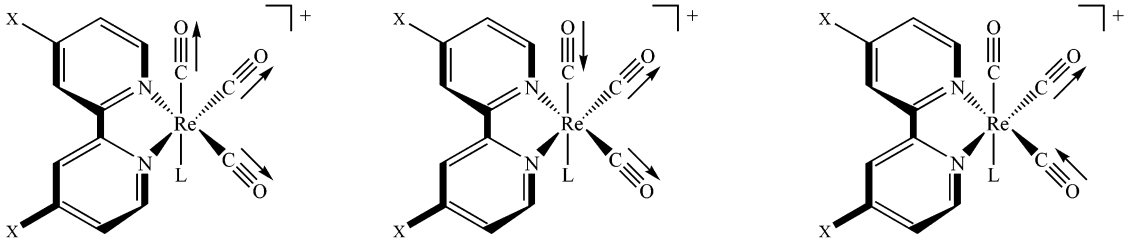

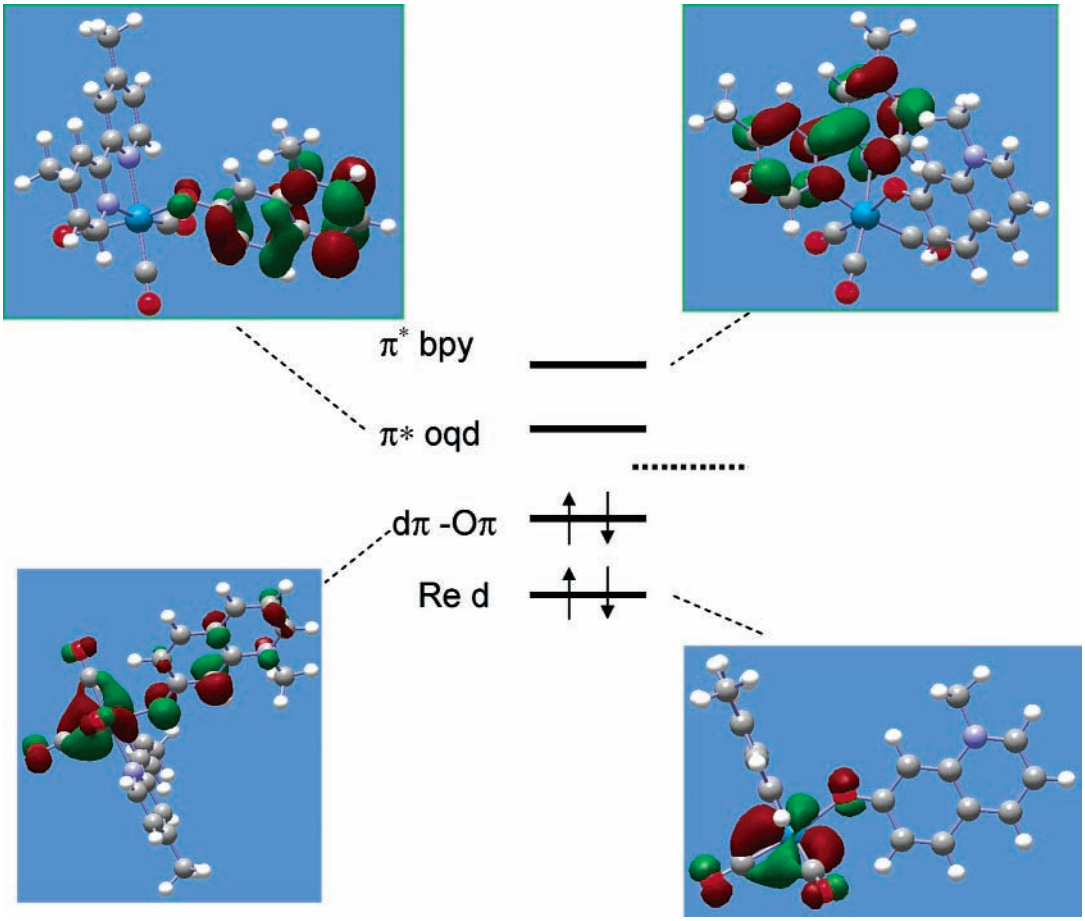


**Figure 5.** DFT-calculated frontier molecular orbital diagrams and relative energies for *fac*-$[Re(CO)_3(bpy)(OQD)]^+$.

**TABLE 3: Summary of TDDFT Calculations on *fac*-$[Re(CO)_3(Me_2dppz)(L)]^+$ Complexes (See Figures 6 and 7)**

| | *E* (eV) | | | | |
|---|---|---|---|---|---|
| state | calcd | expt | orbital excitation | designation | *f* |
| | | | pp = $Me_2$dppz, L = Etpy (**3**) | | |
| $T_1$ | 2.21 | 2.2−2.4[a] | $\pi$ dppz → $\pi_1$* dppz | LC | |
| $T_2$ | 2.63 | | $d_1$ → $\pi_1$* dppz | MLCT | |
| $T_3$ | 2.74 | | $d_2$ → $\pi_1$* dppz | MLCT | |
| $S_1$ | 2.78 | | $d_1$ → $\pi_1$* dppz | MLCT | 0.0016 |
| $S_2$ | 2.80 | | $\pi$ dppz → $\pi_1$* dppz | LC | 0.0672 |
| $S_3$ | 3.03 | | $d_2$ → $\pi_1$* dppz | MLCT | 0.0710 |
| | | | pp = $Me_2$dppz, L = py-PTZ (**4**) | | |
| $T_1$ | 1.62 | | $\pi_2$ ptz → $\pi_1$* dppz | L−L′ | |
| $S_1$ | 1.64 | 1.73[b] | $\pi_2$ ptz → $\pi_1$* dppz | L−L′ | 0.0 |
| $T_2$ | 1.84 | | $\pi_2$ ptz → $\pi_2$* dppz | L−L′ | |
| $S_2$ | 1.84 | | $\pi_2$ ptz → $\pi_2$* dppz | L−L′ | 0.0 |
| $T_3$ | 2.20 | | $\pi_2$ ptz → $\pi_3$* dppz | L−L′ | |
| $S_3$ | 2.20 | | $\pi_2$ ptz → $\pi_3$* dppz | L−L′ | 0.0 |
| $T_4$ | 2.20 | 2.2[b] | $\pi$ dppz → $\pi_1$* dppz | LC | |
| | | >2.2 | | $^3$MLCT | |
| | | <3.2 | | $^1$MLCT | |

[a] Taken from the midpoint of the emission onset (425 nm) and $E_{em}$ = 589 nm and ref 38. [b] Reference 38.

complex **1**; three bands shifted substantially to higher energy relative to the ground state (Figure 2 and Table 1).[6,20,21] In an MLCT excited state, an electron is transferred from a molecular orbital that is largely metal-based to one that is largely ligand-based. This results in a decrease in electron density at the metal, which decreases Re−CO back-bonding, stabilizes the CO $\pi$*, and increases the energy of all three CO stretching modes. The excited-state calculations show that the carbonyl bands retain the same energy ordering in the excited state (A′(1) > A′(2) > A″) with all three bands shifted to higher energy.[34,52] The absolute calculated excited-state vibrational energies are high (no scaling was used), but energy differences between the ground and excited states are comparable to experimental values (30−40 $cm^{-1}$ calculated; 50 $cm^{-1}$ observed).[34,52] The DFT calculations also predict structural changes accompanying excitation as well as intensity changes in excited-state CO bands that lend credence to the notion of $\pi$*(bpy$^{\bullet-}$)−$\pi$*(CO) mixing in the excited state. This study was taken a step further in the accompanying paper by studying the extent of $\pi$*(bpy$^{\bullet-}$)−$\pi$*-(CO) mixing as a function of ground-to-excited-state energy gap in a series of rhenium tricarbonyl complexes.[52]

**d$\pi$−p$\pi$ → $\pi$* Excited States.** The TRIR spectra of *fac*-[Re-$(CO)_3$(4,4′-$(CH_3)_2$bpy)(OQD)]* exhibits the unique pattern of bands shown in Figure 3B, with three bands shifted to higher energy relative to the ground state but to a lesser extent than for comparable MLCT excited states.[46,48] The ground-state symmetry of *fac*-$[Re(CO)_3$(4,4′-$(CH_3)_2$bpy)(OQD)] is $C_s$ due to the nature of the OQD ligand. In the excited state, the $C_s$ symmetry is retained, and the same three bands are observed, though shifted slightly to higher energy. The shifts are smaller than the magnitude typically seen in MLCT states by a factor of $^1/_3$ to $^1/_2$.

A reasonable explanation for this behavior was that the similar excited-state complex, *fac*-$[Re(CO)_3$(4,4′-$(^tBu)_2$bpy)(OQD)]*, is a $\sigma$ → $\pi$* based excited state with an electron promoted from Re−O sigma bond to a polypyridyl based (bpy or OQD) $\pi$* orbital.[37] The DFT calculations point to a related but different description of this excited state. The origin of the HOMO is the Re−O bond, however, it is not of sigma bond character but

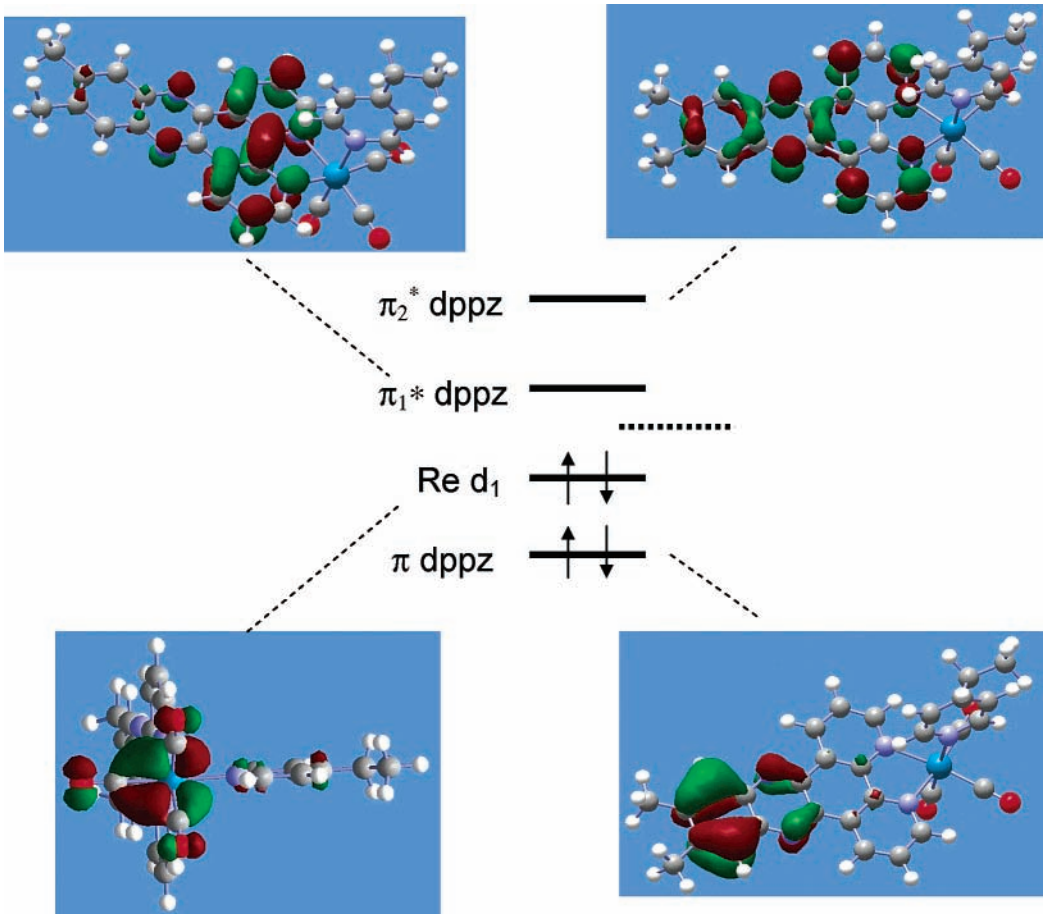


**Figure 6.** DFT-calculated highest-occupied (HOMO) and lowest unoccupied (LUMO) orbitals for *fac*-$[Re(CO)_3(Me_2dppz)(py)]^+$. Also shown is the next lowest lying LUMO orbital, $\pi^*_2$(dppz).

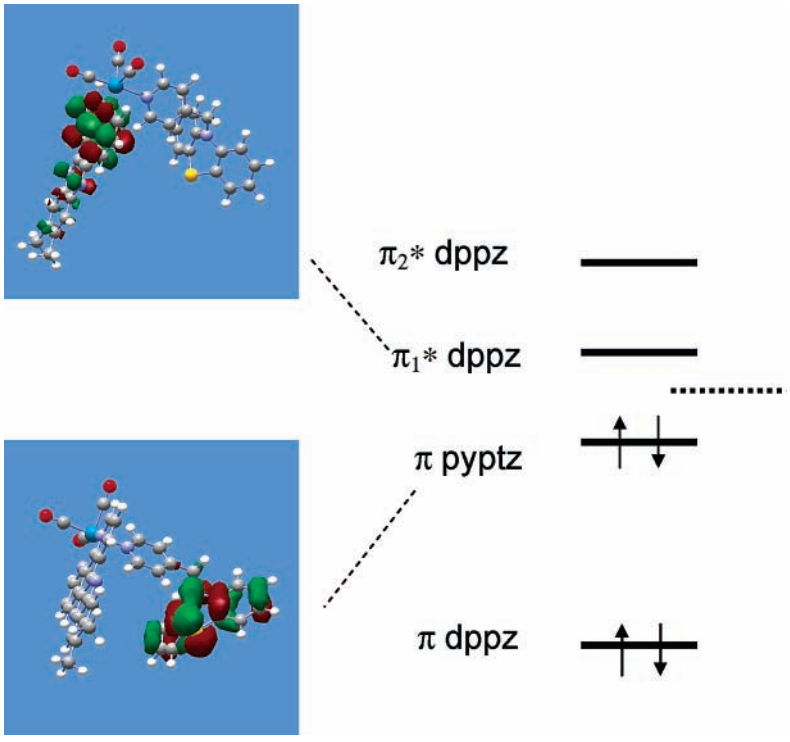


**Figure 7.** DFT-calculated highest-occupied (HOMO) and lowest unoccupied (LUMO) orbitals for *fac*-$[Re(CO)_3(dppz)(py\text{-}PTZ)]^+$. The $\pi$(dppz) orbital, which is also shown schematically, is much lower in energy than indicated in the figure.

rather $\pi$−bonding in nature formed by a d$\pi$(Re)−p$\pi$(O) mixing (Figure 5). The lowest lying unoccupied orbital is on the OQD ligand ($\pi^*$(OQD)) with a closely lying $\pi^*$(bpy) level. This is only true for the lowest triplet. In fact, the lowest lying singlet is (d$\pi$(Re)−p$\pi$(O)) → $\pi^*$(bpy) based. In the lowest excited triplet state of **2**, an electron is promoted from the Re−O $\pi$

orbital to a $\pi^*$ orbital localized on OQD, or ($d\pi$(Re)−p$\pi$(O)) → $\pi^*$(OQD,bpy), with a calculated vertical excitation energy of 2.02 eV (Table 2). The remaining triplet states are ($d\pi$(Re)−p$\pi$(O)) → $\pi^*$(bpy) at 2.37 eV and the MLCT state at 2.63 eV. The transition to the lowest singlet state, $d\pi$(Re)−p$\pi$(O)→$\pi^*$-(bpy) ($S_1$), is at at 2.46 eV. $d\pi$(Re)−p$\pi$(O)→$\pi^*$(OQD) is at 2.68 eV, and the MLCT transition is at 2.89 eV.

The TRIR spectrum of this excited state exhibits three bands, shifted slightly to higher energy relative to the ground state (+4, +17, +28 $cm^{-1}$). This shift to higher energy is indicative of a partial oxidation at the metal and a decrease in electron density at Re available for $\pi$-back-bonding with the carbonyls. In this case, the Re−O(OQD) $\pi$ bond is oxidized which ultimately results in less electron density at $d\pi$(Re) for $\pi$-back-bonding with the carbonyls. In contrast to an MLCT excited state in which there is promotion of an electron from a metal orbital, $d\pi$(Re), to $\pi^*$, less oxidation occurs at Re in this excited state. This is evidenced by the smaller shifts in $\nu$(CO) to higher energy. Partial oxidation causes decreased Re−CO back-bonding, stabilizing CO $\pi^*$, and increased energies for all three CO stretching modes. On the basis of the magnitudes of the shifts, the metal is approximately one-third to one-half as oxidized as in a comparable metal-to-ligand charge-transfer excited state. This assignment is in contrast to the literature[37] and does not account for the purported photoinstability of this complex at the Re−O bond which was speculated to arise from oxidation of the Re−O sigma bond.

**Ligand-Based $\pi \rightarrow \pi^*$ Excited States.** The TRIR spectra of $\pi \rightarrow \pi^*$ excited states exhibit a pattern in which the carbonyl bands shift slightly to lower energy upon excitation.[18−20] The example we present here is *fac*-[Re(CO)$_3$(Me$_2$dppz)(4-Etpy)]$^{+*}$. The small negative shifts of the $\nu$(CO) bands indicate a different excited-state electronic effect. In a $\pi \rightarrow \pi^*$ excited state, an electron is transferred from a bonding orbital which is largely ligand-based to an antibonding orbital which is also largely ligand-based. This antibonding $\pi^*$ orbital is perpendicular to the plane of the polypyridyl ligand, and overlaps with both the metal $d_{xz}$ and $d_{yz}$ orbitals (or, rather, the linear combinations $d_{xz} + d_{yz}$ and $d_{xz} - d_{yz}$).[5] The negative shifts in $\nu$(CO) indicate that there is enhanced mixing with the $d\pi$ orbitals. This increases electron density at $\pi^*$(CO) and weakens the CO bonds in the excited state. This points to increased electron density at the N atoms in the $\pi \rightarrow \pi^*$(dppz) excited state. The $d_{xz}$ and $d_{yz}$ orbitals $\pi$-bond with all three CO ligands. This provides an orbital basis for delocalizing the excited electron over all three CO ligands by $\pi^*$(Me$_2$dppz$^{\bullet-}$)−$\pi^*$(CO) interactions. This causes the $\nu$(CO) shifts to slightly to lower energy.[54,55] $\pi^*$(pp$^{\bullet-}$)−$\pi^*$(CO) interactions also play an important role in the TRIR spectra of other excited states, such as MLCT and redox-separated states, reported here.

The DFT calculations reveal a slight negative shift in $\nu$(CO) in the excited state. The calculated shifts are consistent with the experimental results in predicting that no lowering of symmetry occurs. The two lower energy bands do not separate into a three-band pattern and the symmetry remains pseudo-$C_{3v}$ in the excited state. All the carbonyl bands show approximately equally small negative shifts with no preferential effect.

The small negative shifts of all the carbonyl bands indicate that Re(I) is a better electron donor to CO in the excited state than in the ground state with $^3\pi\pi^*$(Me$_2$dppz) a net electron donor to Re(I) compared to ground-state Me$_2$dppz. In this excited state, slightly more $\pi$-back-bonding exists with the better electron donation.

The DFT calculations capture the near-degeneracy of the low energy $\nu$(CO) bands (only separated by 11 $cm^{-1}$), which also remain close in energy in the excited state. From ground to excited state, DFT calculations also capture the small and negative ground to excited shifts in CO. Not unexpectedly, the absolute gas phase vertical transition energies and magnitudes of CO shifts in the DFT calculations differ, but the calculations adequately predict the ordering of bands and are consistent with the experimental results.

TDDFT calculations (Table 3) were also employed to examine the low-lying triplet and singlet excited states in *fac*-[Re(CO)$_3$(Me$_2$dppz)(4-Etpy)]$^+$. The lowest triplet state ($T_1$) is calculated to be 2.21 eV. This transition involves excitation of an electron from a $\pi$ orbital on the dppz ligand to the lowest $\pi^*$ orbital on the same ligand. Consistent with the experimental results, the calculated lowest excited state is a $\pi\pi^*$(Me$_2$dppz) state. The lowest energy singlet transition, $S_1$, is at 2.78 eV and is attributable to a $d\pi \rightarrow \pi^*$ (MLCT) transition, but $S_2$ arising from $\pi\pi^*$(Me$_2$dppz) is close in energy (2.8 eV) but with a greatly decreased oscillator strength ($f = 0.672$ vs $f = 0.0016$.)

The orbital illustrations of the HOMO and LUMO levels for the complexes add structural information in addition to identifying the nature of the excited state(s). With the dppz ligand being viewed as a combination of phenanthroline and phenazine, $\pi$-(Me$_2$dppz) has electron density localized on the phenazine portion of the dppz ligand. $\pi^*$(Me$_2$dppz) is largely phenanthroline-based with significant coefficients of electron density localized on the N atoms bound to Re. Promotion of an electron into $\pi^*$ should then result in an increase in electron density at the phenanthroline portion of the ligand and the bound N, thus promoting mixing with $d\pi$ and $\pi^*$(CO) as observed experimentally.

**Redox-Separated States.** The TRIR spectra of redox-separated (RS) states typically exhibit the pattern listed in Table 1 for *fac*-[Re$^{\text{I}}$(CO)$_3$(Me$_2$dppz$^{\bullet-}$)(py-PTZ$^{\bullet+}$)]$^{+*}$: two bands, shifted slightly to lower energy relative to the ground state. This state was identified by observing the signature transient feature for PTZ$^{\bullet+}$ at 510 nm in a nanosecond transient absorption experiment described previously.[38,39,50] The transient decayed with $\tau_{RS} \sim 63$ ns ($k \sim 2.0 \times 10^7$ $s^{-1}$).

In the redox-separated state, there is complete reduction at the Me$_2$dppz ligand. The electron added to $\pi$(Me$_2$dppz) interacts with all three CO modes, via $d_{xz}$ and $d_{yz}$ much like the interactions in the $\pi\pi^*$ state mentioned earlier and there is even greater electron density available for mixing. Reduction increases electron density at the N atoms increasing electron density at rhenium by Re−N mixing. This increases $\pi$-back-bonding to CO in the transient RS state. This decreases the energy of the CO bands in the excited state to a greater extent than for $\pi\pi^*$. The "hole" in these complexes, on py-PTZ$^{\bullet+}$, does not affect the electron density on the metal directly because the insulating effect of the methylene spacer between py and PTZ leads to weak electronic coupling.

The energy of $^3\pi\pi^*$(dppz) is ≤2.2 eV based on the highest energy vibronic component in the emission spectrum of **1** and **2**. It is 1.73 eV for the RS state based on the difference between $E_{1/2}$ values for the PTZ$^{+/0}$ and dppz$^{0/+}$ couples by cyclic voltammetry.[38] The DFT calculations predict the lowest excited states $T_1$ and $S_1$ as essentially degenerate with excitation energies of 1.62 and 1.64 eV (Table 3). Two higher ligand to ligand (L−L′) triplet transitions with similar RS character are predicted at 1.84 and 2.20 eV that involve excitations from the same orbital on the py-PTZ ligand to higher $\pi^*$ orbitals on dppz. The intraligand (localized on dppz) $\pi\pi^*$ triplet state ($T_4$) is also

calculated to be the same region at 2.20 eV, in excellent agreement with the experimental value. The corresponding singlet state is not found among the lowest 10 calculated states, however.

As shown in Figure 7, the calculated HOMO is actually the $\pi$ orbital delocalized over the PTZ ligand while the LUMO is a $\pi^*$ orbital localized on the dppz ligand. From the TDDFT results the RS state is predicted to have the "hole" and "electron" localized on the portions of the dppz and PTZ ligands as shown. However, attempts in converging self-consistent DFT calculations and in obtaining an optimized structure for the lowest triplet state encountered difficulties. Depending on the starting guess, self-consistent solutions with comparable energies resembling either a RS state or an intraligand $\pi\pi^*$(dppz) state could be obtained. Consequently, the process of following one of these potential energy surfaces to its respective minimum energy was unsuccessful. We observe that the TDDFT results placed these two states within 0.6 eV in Table 3. These results also confirm the experimental observations of closely spaced, competing excited states discussed previously[38] and in the following section.

**Deconvolution of Competing Excited States.** A final example, complex **5**, is an interesting case because it allows the demonstration of time-dependent deconvolution of signatures from two competing excited states following MLCT excitation in the visible. $Re^I \rightarrow$ dppz excitation at 420 nm is largely MCLT in character producing *fac*-$[Re^{II}(dppz^{\bullet-})(CO)_3(py\text{-}PTZ)]^{+*}$. A competition exists in *fac*-$[Re(CO)_3(dppz)(py\text{-}PTZ)]^+$ between internal conversion to give $^3\pi\pi^*$(dppz), by the transition $(\pi_{dppz})^2(d\pi_{Re})^5(\pi^*_{dppz})^1 \rightarrow (\pi_{dppz})^1(d\pi_{Re})^6(\pi^*_{dppz})^1$, and electron transfer to give the redox-separated (RS) state *fac*-$[Re^I(dppz^{\bullet-})(CO)_3(py\text{-}PTZ^{\bullet+})]^+$, by $(\pi_{PTZ})^2(d\pi_{Re})^5(\pi^*_{dppz})^1 \rightarrow (\pi_{PTZ})^1(d\pi_{Re})^6(\pi^*_{dppz})^1$. The competition ratio is $[RS]/[^3\pi\pi^*] \sim 2.4$, revealing $\pi\pi^*$ as the minor product in the competition.[38]

In the ground-state IR spectrum of *fac*-$[Re^I(dppz)(CO)_3(py\text{-}PTZ)]^+$, two bands arising from the $A_1$ and E modes in $C_{3v}$ symmetry appear at 2037 and 1937 $cm^{-1}$, respectively. The ligands dppz and py-PTZ create an effective local $C_{3v}$ symmetry around $Re^I$ due to their common pyridyl character. Figure 4A shows an average TRIR spectrum in DCE at 298 K from 20 to 300 ns. Figure 4B shows overlaid TRIR spectra taken from averages of short and long time scales.

In the excited state, the two bands shift to lower energy consistent with either RS or $\pi\pi^*$ excited states. As described above, a closely balanced competition exists between these two states. On short time scales (<110 ns), contributions from both RS and $\pi\pi^*$ excited states are expected ($\tau_{RS} \sim 110$ ns), with the RS state being the dominant state at a ratio of 2.4:1. At longer times, the relative population of RS state is dramatically decreased and the resulting TRIR spectrum should represent a mixture with significant $\pi\pi^*$ excited-state character. $\bar{\nu}_{es}$ and correspondingly $\Delta\bar{\nu}$ *do* shift by a small amount with time (Figure 4B). At early sampling times (<300 ns), both the RS state, *fac*-$[Re^I(dppz^{\bullet-})(CO)_3(py\text{-}PTZ^{\bullet+})]^{+*}$ and $\pi\pi^*$ state *fac*-$[Re^I(^3dppz)(CO)_3(py\text{-}PTZ)]^{+*}$ contribute to the TRIR spectrum, although the RS state dominates. Both the frequencies and shifts, $\bar{\nu}_{es} = 1916$ ($\Delta\bar{\nu} = -21$ $cm^{-1}$) and 2028 $cm^{-1}$($\Delta\bar{\nu} = -9$ $cm^{-1}$), are similar to those for the RS state, **4**, at early times. At longer sampling times, $\bar{\nu}_{es} = 1919$ $\Delta\bar{\nu} = -18$ $cm^{-1}$) and 2031 $cm^{-1}$($\Delta\bar{\nu} = -6$ $cm^{-1}$) and the ground-to-excited state shifts are notably smaller. During these time slices, *fac*-$[Re^I(^3dppz)(CO)_3(py\text{-}PTZ)]^{+*}$ is the major contributor to the excited-state spectrum.

Looking at the series of complexes in Table 1, differences in ground-to-excited-state shifts in $\nu$(CO) for RS and $\pi\pi^*$ states can be identified. In comparing *fac*-$[Re^I(Me_2dppz^{\bullet-})(CO)_3(py\text{-}PTZ^{\bullet+})]^{+*}$ and *fac*-$[Re^I(^3Me_2dppz)(CO)_3(4\text{-}Etpy)]^{+*}$, ground-to-excited-state shifts are larger for the RS state. For *fac*-$[Re^I(Me_2dppz^{\bullet-})(CO)_3(py\text{-}PTZ^{\bullet+})]^{+*}$, $\Delta\bar{\nu} = -6$ and $-19$ $cm^{-1}$ while for *fac*-$[Re^I(^3Me_2dppz)(CO)_3(4\text{-}Etpy)]^{+*}$, $\Delta\bar{\nu} = -5$ and $-10$ $cm^{-1}$. The larger shifts for the RS state are due to the increased electronic charge on $Me_2$dppz that is relayed to $\pi^*$-(CO) by $\pi^*(Me_2dppz)$-$d\pi(Re)-\pi^*(CO)$ mixing compared to the $\pi\pi^*$ state.

This is the first example where two competing states have been deconvoluted by using time-dependent TRIR. There is an evolution from RS to $\pi\pi^*$, with $\Delta\bar{\nu}$ decreasing with time due to the decrease in charge on dppz between the RS and $\pi\pi^*$ states which diminishes electron donation into $\pi^*$(CO).

## Conclusions

Combining TRIR and DFT calculations has successfully defined and mapped a series of excited states having significantly different electronic origins. Together, the experiments and calculations are a powerful tool for probing the electronic structures of transient states. This approach has provided an unique interpretation of the *fac*-$[Re^I(CO)_3(4,4'\text{-}(CH_3)_2bpy)(OQD)]$ excited state and predicted the excited-state competition between RS and $\pi\pi^*$ states in *fac*-$[Re^I(CO)_3(dppz)(py\text{-}PTZ)]^+$.

**Acknowledgment.** This work was performed in part at Los Alamos National Laboratory under the auspices of the U.S. Department of Energy and was supported by funds provided by the University of California for the conduct of discretionary research by Los Alamos to J.R.S. D.M.D. acknowledges support from the LANL Director's funded fellowship program. The authors wish to thank Dr. Pingyun Chen for assistance with the spectrum of $[Re(CO)_3(4,4'\text{-}(CH_3)_3bpy)(OQD)]^{+*}$ and Dr. Juan Pablo Claude for the synthesis of this complex. N.L.G. was supported by the University of New Mexico and a DOE Computational Science Graduate Fellowship during her practicum at Los Alamos.

## References and Notes

(1) Omberg, K. M.; Schoonover, J. R.; Meyer, T. J. *J. Phys. Chem.* **1997**, *101*, 9531.
(2) Strouse, G. F.; Schoonover, J. R.; Duesing, R.; Meyer, T. J. *Inorg. Chem.* **1995**, *34*, 2725−2734.
(3) Claude, J. P.; Meyer, T. J. *J. Phys. Chem.* **1995**, *99*, 51−54.
(4) Wallace, L.; Jackman, D. C.; Rillema, D. P.; Merkert, J. W. *Inorg. Chem.* **1995**, *34*, 5210−5214.
(5) Striplin, D. R.; Crosby, G. A. *Chem. Phys. Lett.* **1994**, *221*, 426−430.
(6) Gamelin, D. R.; George, M. W.; Glyn, P.; Grevels, F.-W.; Johnson, F. P. A.; Klotzbucher, W.; Morrison, S. L.; Russell, G.; Schaffner, K.; Turner, J. J. *Inorg. Chem.* **1994**, *33*, 3246.
(7) Johnston, D. H.; Cheng, C.; Campbell, K. J.; Thorp, H. H. *Inorg. Chem.* **1994**, *33*, 6388−6390.
(8) Sacksteder, L. A.; Lee, M.; Demas, J. N. *J. Am. Chem. Soc.* **1993**, *115*, 8230.
(9) Chen, P.; Mecklenburg, S. L.; Duesing, R.; Meyer, T. J. *J. Phys. Chem.* **1993**, *97*, 6811−6815.
(10) Chen, P.; Mecklenburg, S. L.; Duesing, R.; Meyer, T. J. *J. Phys. Chem.* **1993**, *97*, 13126−13131.
(11) Chen, P.; Duesing, R.; Graff, D. K.; Meyer, T. J. *J. Phys. Chem.* **1991**, *95*, 5850−5858.
(12) Worl, L. A.; Duesing, R.; Chen, P.; Della Ciana, L.; Meyer, T. J. *J. Chem. Soc., Dalton Trans.* **1991**, 849−858.
(13) Ruminski, R.; Chambron, R. T. *Inorg. Chem.* **1990**, *29*, 1575−1578.
(14) Tapolsky, G.; Duesing, R.; Meyer, T. J. *Inorg. Chem.* **1990**, *29*, 2285−2297.
(15) Caspar, J. V.; Meyer, T. J. *J. Phys. Chem.* **1983**, *87*, 952−957.
(16) Luong, J. C.; Faltynek, R. A.; Wrighton, M. S. *J. Am. Chem. Soc.* **1980**, *102*, 7892−7900.

(17) Wrighton, M. S.; Morse, D. L. *J. Am. Chem. Soc.* **1974**, *96*, 998−1003.
(18) Schoonover, J. R.; Bignozzi, C. A.; Meyer, T. J. *Coord. Chem. Rev.* **1997**, *165*, 239−266.
(19) Schoonover, J. R.; Strouse, G. F.; Dyer, R. B.; Bates, W. D.; Chen, P.; Meyer, T. J. *Inorg. Chem.* **1996**, *35*, 273−274.
(20) Schoonover, J. R.; Strouse, G. F.; Omberg, K. M.; Dyer, R. B. *Comments Inorg. Chem.* **1996**, *18*, 165.
(21) Turner, J. J.; George, M. W.; Johnson, F. P. A.; Westwell, J. R. *Coord. Chem. Rev.* **1993**, *125*, 101.
(22) Schoonover, J. R.; Gordon, K. C.; Argazzi, R.; Woodruff, W. H.; Peterson, K. A.; Bignozzi, C. A.; Dyer, R. B.; Meyer, T. J. *J. Am. Chem. Soc.* **1993**, *115*, 10996−10997.
(23) Glyn, P.; George, M. W.; Hodges, P. M.; Turner, J. J. *J. Chem. Soc., Chem. Commun.* **1989**, 1655.
(24) Brisdon, B. J.; Edwards, D. A.; White, J. W. *J. Organomet. Chem.* **1978**, *156*, 427−437.
(25) Wuyts, L. F.; Van Der Kelen, G. P. *Inorg. Chim. Acta* **1977**, *23*, 19−22.
(26) Dalton, J.; Paul, I.; Smith, J. G.; Stone, F. G. A. *J. Chem. Soc. A* **1968**, 1208−1211.
(27) Houk, L. W.; Dobson, G. R. *Inorg. Chem.* **1966**, *5*, 2119−2123.
(28) Larsen, E.; Mason, S. F. *J. Chem. Soc. A* **1966**, 313−315.
(29) Cotton, F. A.; Kraihanzel, C. S. *J. Am. Chem. Soc.* **1962**, *84*, 4432−4438.
(30) Hay, P. J. *J. Phys. Chem. A.* **2002**, *106*, 1634.
(31) Rosa, A.; Baerends, E. J.; vanGisbergen, S. J. A.; vanLethe, E.; Gooneneveld, J. A.; Snijders, J. G. *J. Am. Chem. Soc.* **1999**, *121*, 10356.
(32) Adamo, C.; Barone, V. *Theor. Chem. Acc.* **2000**, *105*, 169.
(33) Boulet, P.; Chermett, H.; Daul, C.; Gilardoni, F.; Roogenond, F.; Weber, J.; Zuber, G. *J. Phys. Chem. A* **2001**, *105*, 885.
(34) Dattelbaum, D. M.; Omberg, K. M.; Schoonover, J. R.; Martin, R. L.; Meyer, T. J. *Inorg. Chem.* **2002**, *41*, 6071−6079.
(35) Farrell, I. R.; vanSlageren, J.; Zalis, S.; Vlcek, A. *Inorg, Chim. Acta* **2001**, *315*, 44.
(36) Lopez, L. In *Chemistry*; Pontificia Universidat Catolica de Chile: Santiago, Chile, 1994.
(37) Claude, J. P.; Omberg, K. M.; Williams, D. S.; Meyer, T. J. *J. Phys. Chem. A* **2002**, *106*, 7795. Claude, J. P.; Williams, D. S.; Meyer, T. J. *J. Am. Chem. Soc.* **1996**, *118*, 9782.
(38) Bates, W. D.; Chen, P. Y.; Dattelbaum, D. M.; Jones, W.; Meyer, T. J. *J. Phys. Chem. A* **1999**, *103*, 5227−5231.
(39) Chen, P. Y.; Westmoreland, T. D.; Danielson, E.; Schanze, K. S.; Anthon, D.; Neveux, P. E.; Meyer, T. J. *Inorg. Chem.* **1987**, *26*, 1116.
(40) Omberg, K. M.; Schoonover, J. R.; Treadway, J. A.; Leasure, R. M.; Dyer, R. B.; Meyer, T. J. *J. Am. Chem. Soc.* **1997**, *119*, 7013−7018.
(41) Dattelbaum, D. M.; Meyer, T. J. *J. Phys. Chem. A* **2002**, *106*, 4519−4524.
(42) (a) Becke, A. D. *J. Chem. Phys.* **1993**, *98*, 1372. (b) Frisch, M. J.; Trucks, G. W.; Schlegel, H. B.; Scuseria, G. E.; Robb, M. A.; Cheeseman, J. R.; Zakrzewshi, V. G.; Montgomery Jr., J. A.; Stratmann, R. E.; Burant, J. C.; Dapprich, S.; Millam, J. M.; Daniels, A. D.; Kudin, K. N.; Strain, M. C.; Farkas, O.; Tomasi, J.; Barone, V.; Cossi, M.; Cammi, R.; Mennucci, B.; Pomelli, C.; Adamo, C.; Clifford, S.; Ochterski, J.; Petersson, G. A.; Ayala, P. Y.; Cui, Q.; Morokuma, K.; Malick, D. K.; Rabuck, A. D.; Raghavachari, K.; Foresman, J. B.; Cioslowski, J.; Ortiz, J. V.; Baboul, A. G.; Stefanov, B. B.; Liu, G.; Liashenko, A.; Piskorz, P.; Komaroni, I.; Gomparts, R.; Martin, R. L.; Fox, D. J.; Keith, T.; Al-Laham, M. A.; Peng, C. Y.; Wong, M. W.; Andres, J. L.; Gonzolez, C.; Head-Gordon, M.; Replogle, E. S.; Pople, J. A. Gaussian Inc.: Pittsburgh, PA, 1998.
(43) Hay, P. J.; Wadt, W. R. *J. Chem. Phys.* **1995**, *82*, 299.
(44) Bauernschmitt, R.; Ahlrichs, R. *Chem. Phys. Lett.* **1996**, *256*, 454.
(45) Stratmann, R. E.; Scuseria, G. E.; Frisch, M. J. *J. Chem. Phys.* **1998**, *109*, 8218.
(46) Stufkens, D. J.; Vlcek, A., Jr. *Spectrum* **1996**, *9*, 2−7.
(47) Rossenaar, B. D.; Stufkens, D. J.; Vlcek, A. J. *Inorg. Chem.* **1996**, *35*, 2902−2909.
(48) Rossenaar, B. D.; George, M. W.; Johnson, F. P. A.; Stufkens, D. J.; Turner, J. J.; Vlcek, A., Jr. *J. Am. Chem. Soc.* **1995**, *117*, 11582−11582.
(49) Schoonover, J. R.; Strouse, G. E. *Chem. Rev.* **1998**, *98*, 1335−1355.
(50) Maxwell, K. M.; Sykora, M.; DeSimone, J. M.; Meyer, T. J. *Inorg. Chem.* **2000**, *39*.
(51) Dattelbaum, D. M. Unpublished results.
(52) Dattelbaum, D. M.; Martin, R. L.; Schoonover, J. R.; Meyer, T. J. *J. Phys. Chem. A*, submitted for publication.
(53) Cotton, F. A. *Chemical Applications of Group Theory.*; John Wiley & Sons: New York, 1990.
(54) Schoonover, J. R.; Bates, W. D.; Meyer, T. J. *Inorg. Chem.* **1995**, *34*, 6421.
(55) Schoonover, J. R.; Bates, W. D.; Strouse, G. F.; Chen, P.; Dyer, R. B.; Meyer, T. J. *Inorg. Chem.* **1995**, *35*, 473.